## CONFERENCE PRE-PRINT

## FORMATION OF THE HFSHD AT GLOBUS-M2 TOKAMAK

E.E. MUKHIN, N.V. ERMAKOV, N.S. ZHILTSOV, G.S. KURSKIEV, S.YU. TOLSTYAKOV, E.E. TKACHENKO, V.A. TOKAREV, V.A. SOLOVEY., N.A. KHROMOV, E.O. KISELEV, A.N. KOVAL, K.O. NIKOLAENKO, A.N. NOVOKHATSKY, YU.V. PETROV, N.V. SAKHAROV, P.B. SHCHEGOLEV, A.YU. TELNOVA, E.A. TUKHMENEVA

**Ioffe Institute** 

St.Petersburg, Russian Federation Email: e.mukhin@mail.ioffe.ru

E.G. KAVEEVA, K.A. KUKUSHKIN, I.YU. SENICHENKOV, V.A. ROZHANSKY Peter the Great St. Petersburg Polytechnic University

St.Petersburg, Russian Federation

A.A. KAVIN Efremov Institute St.Petersburg, Russian Federation

#### Abstract

The paper presents the development of a region of High Field Side High Density Region (HFSHD) in the lower inner divertor of the Globus-M2 tokamak (R=0.36 m, a=0.24 m). Discharges with NBI heating (0.7 MW) were investigated using two Thomson scattering diagnostics with probing chords situated at inner divertor near X-point and in outer midplane near separatrix. Maximum electron density in the inner divertor leg was found to be 1.5-3 times higher than the density at the outer midplane plasma boundary. The HFSHD region is formed for a wide range of parameters with electron density at the magnetic axis in the range from 2  $10^{19}$  to  $1.4 \, 10^{20}$  m<sup>-3</sup>. This experimental program was supported by SOLPS-ITER modelling with account of drifts and currents. The neutral particle behaviour was modelled with the EIRENE neutral gas transport Monte Carlo code taking into account deuterium atoms, molecules and carbon atoms.

# 1. INTRODUCTION

Here we report on the formation of the HFSHD regime observed at Globus-M2 (equipped with full C walls) in scenarios with both ohmic heating and NBI heating (0.4 MW): with the central n\_e varying from 2 1019 to 1.4 1020 m-3. The yielded data show presence of high n\_e region within inner divertor of the Globus-M2 tokamak, exceeding n\_e on a same magnetic surface in the outer midplane by a factor of 1.5-3 (see Fig. 7). The experimental results allow us to make an assumption about stability of the HFSHD phenomenon in spherical tokamaks with carbon walls. Furthermore, a joint analysis of multiple subsequent measurements revealed that the movement of the separatrix did not result in modifying the divertor operational mode.

This phenomenon was also confirmed in modelling with the SOLPS-ITER code [1] accounting drifts and currents, where the EIRENE Monte-Carlo description of deuterium atoms/molecules and carbon atoms was used. The simulation showed a clearer manifestation of the HFSHD phenomenon compared to the previous GLOBUS-M and GLOBUS-M2 modelling [2-4], where motion of neutrals was described with fluid approach.

# 2. EXPERIMENTAL SETUP

Globus-M2 is a spherical tokamak with small aspect ratio (R = 0.36 m, a = 0.24 m, R/a = 1.5). In the experiments discussed, toroidal magnetic field and plasma current were varied within the range of 0.7 - 0.8 T, and of 0.3 - 0.35 MA, respectively. Figure 1 shows the typical magnetic configuration reconstructed for the shot #44644 and Globus-M2 vacuum chamber with midplane TS and divertor TS probing points, IR camera field of view and positions of Langmuir probes.

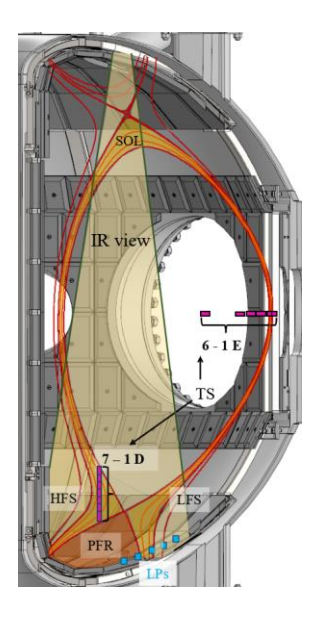


FIG. 1. Globus-M2 vacuum chamber and typical magnetic configuration (shot #44644). Blue dots (LPs) show locations of the Langmuir probes. Light cone - field of view of IR camera. The red rectangles - Thomson scattering (TS) diagnostic spatial channels. HFS, LFS, and PFR - the high-field side, low-field side, and private flux regions, respectively.

The divertor electron parameters were measured by the divertor Thomson scattering diagnostics (DTS) [5], with vertical probing chord passing at R=24 cm through the High Field Side area near X-point. The scattered radiation was collected from seven spatial points, with resolution of ~12 mm. In different discharges, the DTS measurement position relative to the normalized flux surface coordinates varied in the range  $\rho_{\psi} \in [0.95, 1.05]$ . Measurements of  $n_e$ ,  $T_e$  by helium imaging spectroscopy diagnostic in this region showed comparable results [6].

In the midplane, the electron parameters in both core and edge regions were measured along the midplane probing chord in six spatial points. The DTS probing laser parameters [7] are as follows: Nd:YAG 1064 nm/2 J/100 Hz/3 ns. AR-coated lens (f=2 m) focuses DTS laser beam forming a waist of ~3 mm in diameter along the probing chord of 100 mm. Parameters of the Nd:YAG laser used for the midplane TS are as follows: 1064 nm/3 J/330 Hz/10 ns [8]. Synchronization of the midplane and DTS lasers was achieved with an accuracy of 0.1 ms, ensuring temporal coincidence of every third shot of the midplane laser with shots of the DTS laser. The discharge duration of 100 milliseconds provided stable plasma parameters during approximately 50 milliseconds, allowing up to five measurements per discharge at the DTS repetition rate 100 Hz.

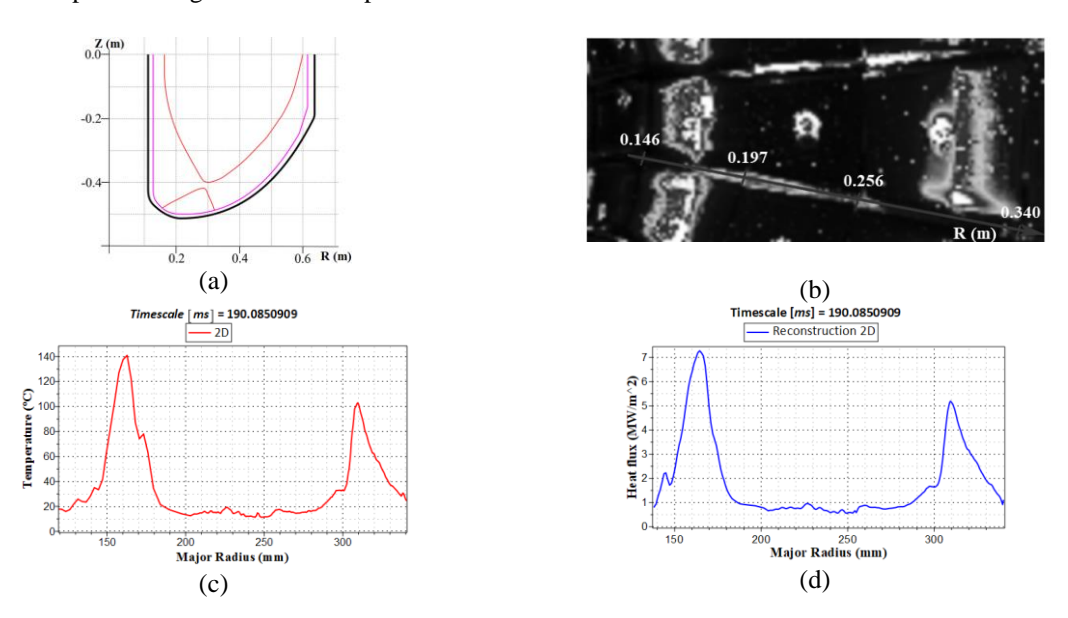


FIG. 2. Discharge #44644 IR camera analysis. (a) Separatrix at 183 ms; (b) IR camera image of inner and outer strike points; (c) Temperature distribution; (d) Estimated heat flux density distribution.

To reconstruct the plasma shape boundary in Globus-M2 the current filament method [9] is routinely used. Since this method is not suitable for simulation of poloidal magnetic flux evolution, as well as other key metrics such as poloidal beta, internal inductance and so on, the Globus-M2 team has developed a free-boundary equilibrium code pyGSS [10]. The pyGSS code was verified by comparing the simulation results with the PET code [11, 12] with a MAPE (mean absolute percentage error) of 11% (when comparing poloidal beta, internal inductance and stored energy). The elongation as well as the minor and major radii determined by the current filament method and by the pyGSS code, were found to agree with each other with a MAPE < 2%. The pyGSS simulation results were compared with the measurements carried out by diamagnetic loops that was not used in the reconstruction (MAPE of 8.6%).

## 3. EXPERIMENTAL

In 2024 experimental campaign (at both Ohmic (OH) and NBI heating with B  $\sim$  0.7 T, I  $\sim$ 300-350 kA), the typical scenario was characterized by formation of the divertor configuration at 160 ms, following a noticeable increase of ne at the high-field side (HFS) of divertor, while ne on separatrix in middle plane remained constant. Figure 3 shows time traces of main parameters for the typical discharge #44644 with applied 0.7 MW NBI heating chosen for the detailed analysis.

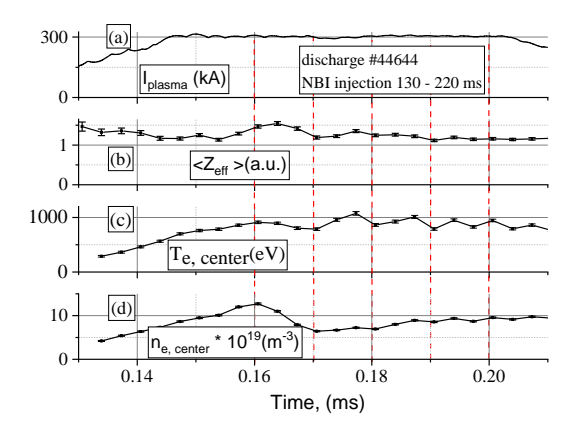


FIG. 3. Parameters of discharge #44644 (a) Plasma current  $I_p$ , (b) <Z<sub>eff</sub>>, (c) central  $T_e$  measured by TS, (d) central  $n_e$  measured by TS.

The quasi-stationary phase of the discharge (160 - 200 ms) was selected for further consideration. The red lines indicate timestamps of the DTS laser shots. Figure 4a illustrates formation of the divertor magnetic configuration from 160 ms to 200 ms. The magnetic configuration at 160 ms is appropriate for comparison of DTS and midplane TS data on the same closed magnetic surfaces.

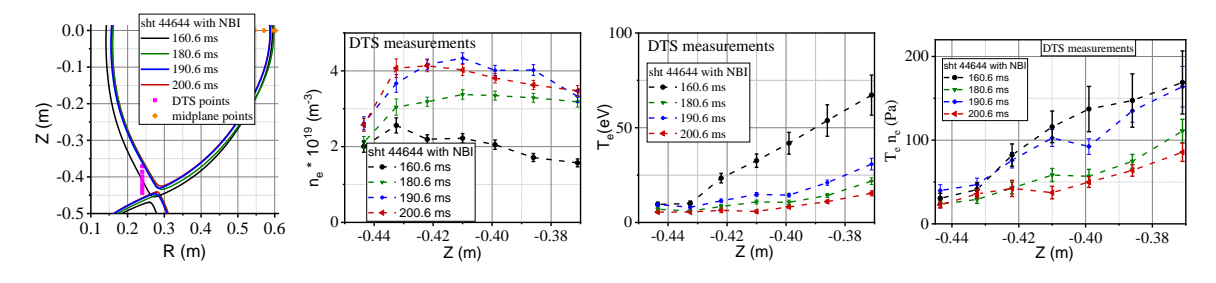


FIG. 4. Position of separatrix for the shots #44613 and #44644; location of midplane TS and DTS probing points and Profiles of  $n_e$ ,  $T_e$  and  $p_e$  measured by DTS at 160.6, 180.6, 190.6 ms and 200.6 ms in discharges #44613 and #44644.

Figures 4 b show inherent evolution of the electron parameters along the DTS probing chord. The figure shows that at a distance of 5 cm from the separatrix, the electron pressure decreases by 3-4 times. At the same time, the electron density remains constant. Figure 5 shows comparison of  $n_e$ ,  $T_e$  and  $p_e$  profiles measured by DTS and midplane TS plotted as a function of the normalized poloidal magnetic flux, defined as  $\rho_{\psi}$  =

 $\sqrt{(\psi - \psi_0)/(\psi_I - \psi_0)}$ , where  $\psi$  is the poloidal magnetic flux,  $\psi_0$  and  $\psi_I$  correspond to the magnetic axis and the sepatrix, respectively.

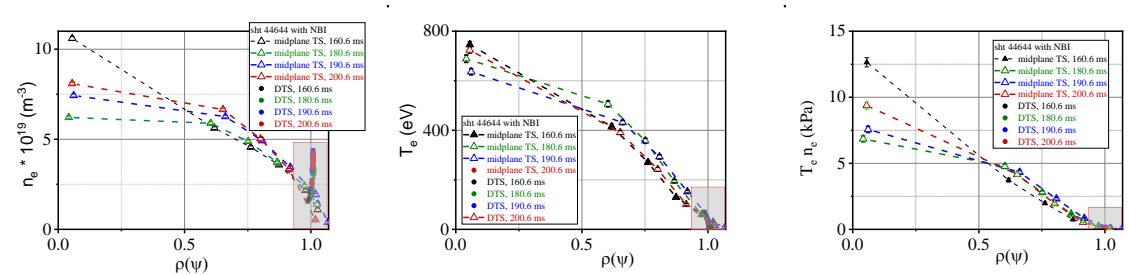


FIG. 5.  $n_e$ ,  $T_e$  and  $p_e$  measured by DTS and midplane TS as a function of the normalized poloidal magnetic flux  $\rho_{\psi}$ . The experimental points mark centres of TS spatial channels. The red rectangles indicate areas zoomed in Figure 6(a) and 6(b).

Note that the profiles measured on the same flux surfaces in the divertor and midplane are in good agreement when a part of DTS probing chord is situated within the area of confinement at the stage of divertor configuration formation (see Figure 6a). However, at 180-200 ms (Figure 6b), the DTS probing chord is shifted outside the separatrix, where the arrangement of DTS spatial channels along one magnetic surface exhibited a region of increased  $n_e$ .

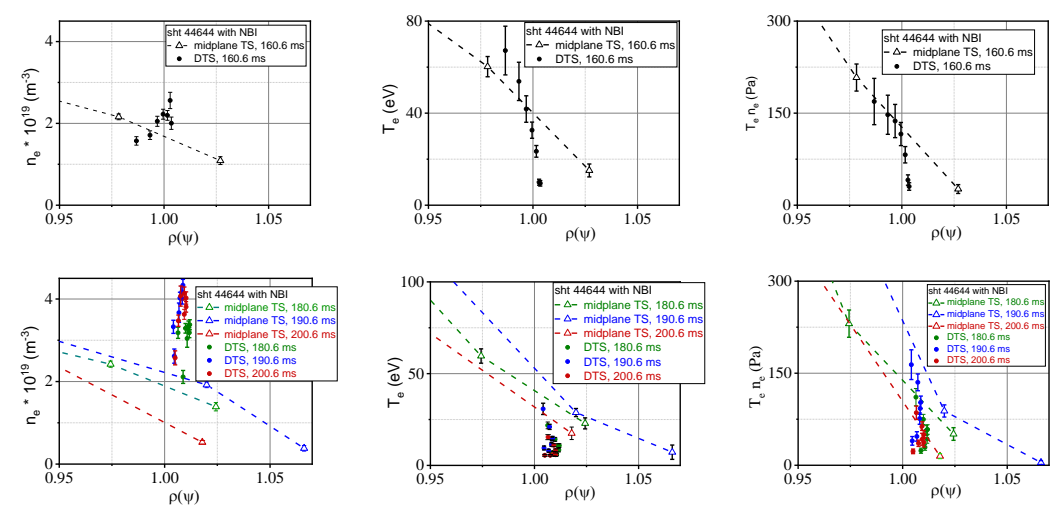


FIG. 6.  $n_e$ ,  $T_e$  and  $p_e$  at 160 ms, when several DTS points are situated within the plasma confinement region (upper row) and the profiles measured at 180 ms, 190 ms and 200 ms (lower row).

TS measurements during quasi-stationary phase of 18 discharges (with both OH and NBI heating) demonstrate that the maximum density in the inner divertor leg is 1.5-3 times higher than the density at the outer midplane plasma boundary. We associate this effect with formation of the HFSHD region. Figure 7a shows dependence of  $n_e$  at the plasma center (coloured) and on the separatrix measured by the midplane TS as a function of the maximum ne measured by DTS. Figures 7b and 7c show  $T_e$  and  $p_e$  behaviour for the DTS spatial points where the maximum  $n_e$  were measured.

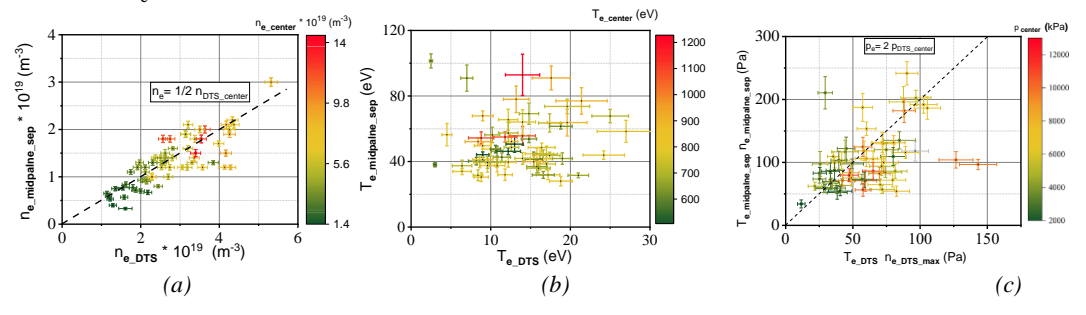


FIG. 7. TS measurements during quasi-stationary phase of 18 discharges (with both OH and NBI heating).  $a - n_e$  at the plasma center (colored) and on the separatrix (vertical axis) measured by midplane TS as a function of the maximum  $n_e$  measured by DTS,  $b - T_e$  at the plasma center (colored) and on the separatrix measured by midplane TS as a function of  $T_e$  measured by DTS at the point of maximum  $n_e$ ,  $c - p_e$  at the plasma center (colored) and on the separatrix measured by midplane TS as a function of  $p_e$  measured by DTS at the point of maximum  $n_e$ .

## 4. MODELING RESULTS

The detected formation of a region characterized by high ne in the Globus-M2 inner divertor has been confirmed by means of simulations using the SOLPS-ITER code [1] done with full account of drifts and currents. The grad B drift of ions is directed towards the active X-point. The simulation was performed for the discharge #44644 (see Figure 3).

The neutral component, comprising deuterium atoms and molecules, as well as carbon atoms, was modelled using a Monte Carlo numerical approach with the EIRENE code. Taking into account the large mean free paths of neutral particles in comparison to characteristic scales of the plasma parameters in Globus-M2 the Monte-Carlo modeling gives a substantial enhancement in accuracy in comparison with the hydrodynamic approach [12-14]. This approach enables more precise calculation of the ionization source, both inside and outside the separatrix. EIRENE modeling region spans up to the chamber wall facilitating the accurate description of neutral particles in the geometry of the Globus-M2, including the position of the deuterium inlet. The deuterium puffing position and value correspond to the experimental ones. The gas puffing rate is  $3 \cdot 10^{20}$  atoms/s. The flow of deuterium from the core corresponding to the NBI in modeling is  $1.1 \cdot 10^{20}$  atoms/s, which is considerably smaller than the ionization source in the modeling region inside the separatrix. Globus-M2 discharge duration is shorter than typical time scales of ~1 s required for saturation with deuterium of the first wall surfaces. Therefore, it was assumed in the simulation that a process of partial absorption of deuterium would occur on the divertor plates and on the first wall. The steady-state density level in the simulation was obtained with a reflection coefficient of hydrogen incident on the surface equal to 99.3%. Presence of carbon impurity was accounted for in the simulation. The physical sputtering of carbon was calculated using the Roth-Bohdansky equation [13, 14]. Constant chemical sputtering yield for carbon atoms outflow from surfaces equal to 8% of deuterium atoms and ions flow to surfaces was imposed. This enabled the calculated value of the effective charge at the inner boundary of the computational domain to be aligned with the experimental results. The calculation was made under the standard for such modeling assumption that there is no reflection of incident carbon ions and atoms, and that they are completely absorbed on all surfaces. At the inner boundary of the computational domain, the carbon flux into the plasma, calculated as the sum of all charge states, was assumed to be zero. The calculated effective charge value was determined to be 1.3 at the inner boundary of the computational domain and 1.9 at the separatrix on the outer midplane. The average calculated carbon density at the separatrix has been found to be  $9.5 \cdot 10^{17} \text{m}^{-3}$ .

The mesh for modeling is shown in Figure 8(a). In contrast to the discharges in the simulations [2-4], the discharge #44644 has an increased distance between the active separatrix on the inner midplane and the central column, as well as the distance between the separatrix on the outer midplane and the chamber wall. This configuration increasing the width of the scrape-of-layer (SOL) makes it possible to increase the computational domain at expense of decreasing the main plasma volume. The increased SOL width provides almost complete protection of the wall from the energy flux from the core plasma. The total width of the computational domain outside the active separatrix on the outer midplane is approximately 21 mm. The heat fluxes from the central region were specified with account of the ohmic heating power  $(P_{ohm})$  of 290 kW and the neutral injection heating  $(P_{NBI})$  of 410 kW. The distance between the active and passive separatrices on the outer midplane was approximately 4.2 mm. The choice of transport coefficients, see Figure 8(b), facilitated good agreement of electron density and temperature profiles in the outer midplane with the measured values, (see Figure 8 c, d). Comparison of the target profiles obtained in the modeling and measured experimentally is shown in Fig.8(e,f). The saturation current fits well, while the modeling underestimates the target temperature by a factor of two. It can be associated with kinetic effects in the electrons distribution due to big mean free path of electrons comparing to the distance between the outer midplane and outer target of Globus-M2 or with dynamic effects due to ELMs bursts not included in the modeling. Additionally, such a discrepancy between experimental and simulation data may arise from specific features of the computational mesh in the SOLPS-ITER code (version 3.0.8). In this version of the code, the mesh for fluid modeling of plasma covers only a portion of the tokamak chamber, being limited to surfaces continuously connecting the divertor plates (Fig.8(a)). Consequently, the difference between the measured and simulated electron temperatures could be attributed to the unaccounted influence of regions not covered by the mesh.

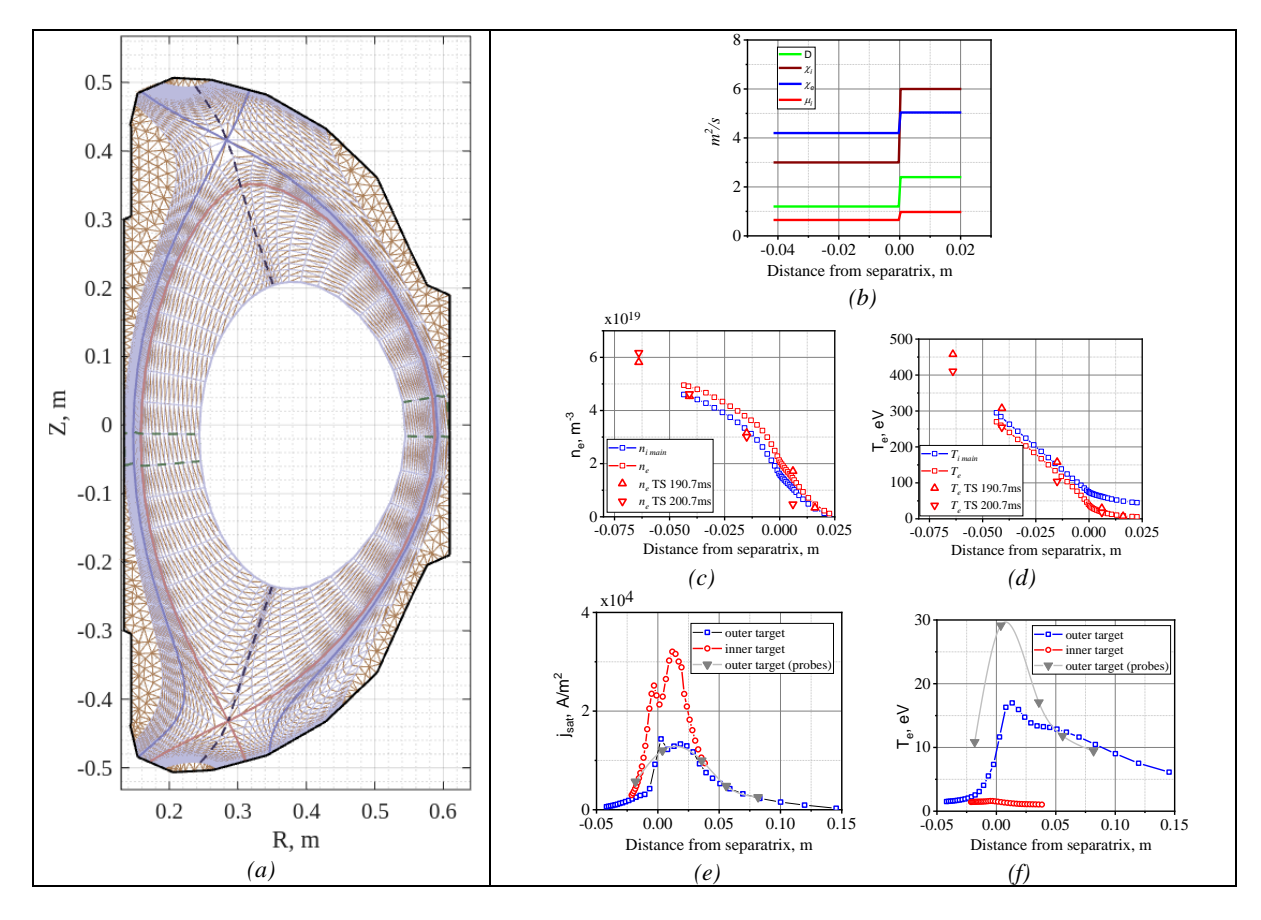


FIG. 8. (a) SOLPS-ITER plasma (blue) and EIRENE (dark yellow) meshes; (b) anomalous transport coefficients: diffusion coefficient D, electron and ion thermal conductivities  $\chi_e, \chi_i$ , viscosity coefficient  $\mu_{\perp}$ ; (c) Density and (d) temperature of electrons and ions at outer midplane; (e) Saturation current and (f) electron temperature at the lower divertor targets.

The simulated two-dimensional electron density and temperature distributions in divertor region and comparison of the measured by DTS and the modeled temperature and density profiles are shown in Figure 9. Distribution of the simulated saturation currents for all divertor targets are compared with probe measurements in Figure 10. The simulation generally supports the conclusion of [4] regarding the formation of a region of increased  $n_e$  and decreased  $T_e$  in the divertor on the side of the strong magnetic field in Globus-M2. The modeled values of density and temperature at the outer midplane at the same flux tubes as measured by DTS are also shown in Fig. 9. It is seen that in the modeling the temperature of electrons is approximately twice smaller and the density is twice bigger in the divertor than at the midplane. The increased density region is located between the active and inactive separatrices, where the cold upper inner target is connected by magnetic tubes with the hot lower inner target. This connection leads to the thermoelectric current, directed towards target in the inner divertor. Poloidal electric field directed towards the target is required for the thermoelectric current to pass through the inner divertor cold plasma layer. Moreover, the electron temperature and pressure are big in this region arranged at the X-point level giving rise to Boltzmann and thermal force contributions to the potential variation. All these effects lead to the elevated electrostatic potential at the X-point level between the separatrices and to the corresponding electric field. In contrast, in the far SOL beyond the inactive separatrix the thermoelectric current, the electron temperature and density and their variations are low. Therefore, the regions of high electric field and corresponding drifts are all localized between the separatrices. The radial ExB drift of ions and electrons in the direction of the strong magnetic field leads to the formation of a region of increased density. The mechanism is similar to that in ASDEX Upgrade [4]. The distribution of the electrostatic potential in the divertor region together with the directions of ExB and grad B ions flows are shown in Figure 11. It is interesting to note that, in the case of Globus-M2 (in contrast to the ASDEX Upgrade case), the grad B drift contributes significantly to plasma transport through the separatrix below the X-point. As it is found in the simulation, grad B drift flow through the separatrix is approximately twice smaller by absolute value than the flux associated with the ExB drift for the inner divertor leg, and equals to approximately 30% of ExB flux in the outer divertor. In both divertors, this grad B flux is directed towards the private flux region (PFR), thereby reducing the effect of electric drift in formation of the high-density region. The total drift flux (including the contributions of the ExB and grad B drifts) through the separatrix of the inner divertor

equals to approximately 50% of the ion flux to the inner target between the separatrices, thus significantly changing the particle balance in the inner divertor region.

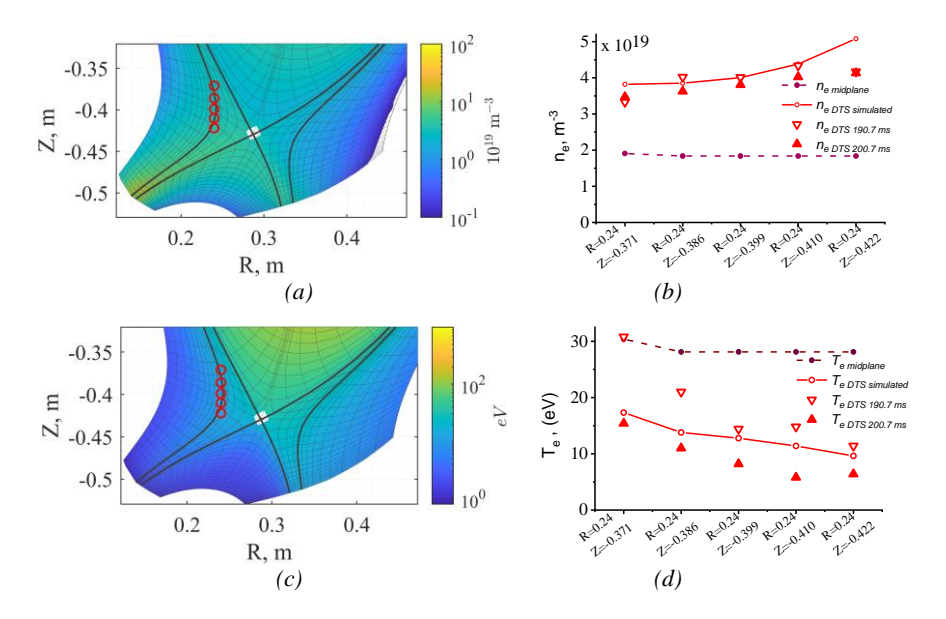


FIG. 9. Comparison of the modeled temperature and density profiles with the profiles measured by DTS. (a) 2D plot of electron density and (b) comparison of density to DTS measurements; (c) 2D plot of electron temperature and (d) comparison of temperature to DTS measurements. DTS measurements points are marked in 2D plots (c) by red circles.

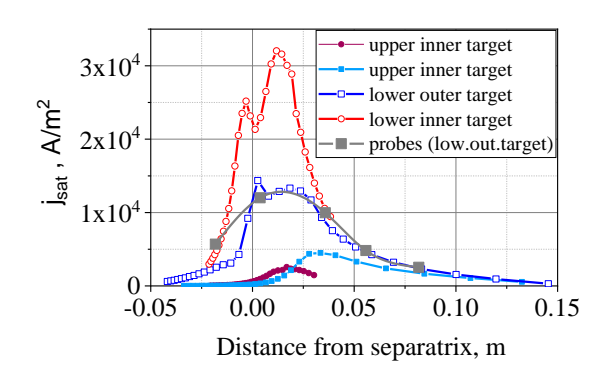


FIG. 10. Saturation current calculated for divertor targets compared with probe measurements.

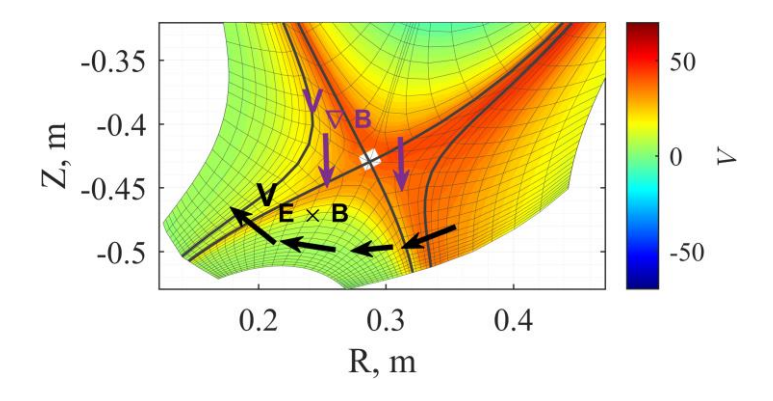


FIG. 11. Map of electrostatic potentials and directions drift flows in divertor region.

#### 5. CONCLUSION

The paper presents first results of divertor plasma systematic study in Globus-M2 tokamak supported by SOLPS-ITER simulation with a description of the neutral component by the Monte Carlo method. The set of diagnostic systems includes two Thomson scattering diagnostics with probing chords located in the lower divertor from the high-field side and in the edge of outer midplane, IR video camera with an overview of the outer and inner strike points of the lower divertor and Langmuir probes located on the outer divertor target. High Field Side High Density (HFSHD) previously discovered on DIIID, JET and ASDEX has now been discovered in spherical tokamak Globus-M2 with C walls. This was observed during quasi-stationary phase of 18 discharges over a wide range of discharge parameters, with the central ne changing in the range from 2×10<sup>19</sup> to 1.4×10<sup>20</sup> m<sup>-3</sup>, both with and without deuterium neutral beam injection (0.7 MW). Measurements of the divertor Thomson scattering show formation of a plasma region with increased ne, maximized at a distance of ~3 cm from X-point and ~2 cm from the separatrix. Maximum ne values measured in inner divertor leg exceeds by 1.5-3 times ne on the same magnetic surface measured in the outer equatorial plane. This experimental data showed agreement with simulation made for the discharge #44644 using the SOLPS-ITER code with a description of deuterium atoms, molecules and carbon atoms, employing the EIRENE code with the Monte Carlo approach. Identification of HFSHD phenomenon in spherical tokamak is important for enhanced knowledge of the plasma stability mechanisms in tokamaks of this type, and for improving control and optimization of plasma regimes in future machines like a reactor-scale spherical tokamak. Further work is planned to be directed towards studying the influence of various radiants and changes in distance between active and passive separatrices on the HFSHD formation and plasma behaviour in both X-point and private flux regions.

#### **ACKNOWLEDGEMENTS**

Work on the study of divertor plasma was supported by the Russian Science Foundation (23-79-00033).

## REFERENCES

- [1]. X. BONNIN, et al Presentation of the new SOLPS-ITER code package for tokamak plasma edge modelling, Plasma Fusion Res. **11** (2016) 1403102.
- [2]. E. VEKSHINA, et al, Modelling of Globus-M connected double null discharge, Plasma Phys. Control. Fusion **61** (2019) 125009.
- [3]. E. VEKSHINA, et al., Experiment with nitrogen seeding at the Globus-M2 tokamak, Phys. Plasmas 30 (2023) 042504.
- [4]. K. DOLGOVA, et al, Modelling of high-field-side high-density regime in the Globus-M2 tokamak, Plasma Phys. Control. Fusion **66** (2024) 035001.
- N. ERMAKOV et al, Divertor Thomson Scattering on Globus-M2, Plasma Physics Reports 49 (2023) Issue 12, p.1480-1489.
- [6]. D.D. KOROBKO et al., Measurement of electron concentration and temperature in the Globus-M2 tokamak SOL using helium imaging spectroscopy (2025), *to be published*.
- [7]. E.E. MUKHIN et al., The ITER divertor Thomson scattering system: engineering and advanced hardware solutions, JINST **7** (2012) C02063.
- [8]. G.S. KURSKIEV et al., Electron temperature measurements at the Globus-M2 tokamak using multi-laser Thomson scattering, Technical Physics Letters **48** (2022) Is.15 78-82.
- [9]. V.I. VASILIEV et al, On-line plasma shape reconstruction algorithm in tokamaks and its verification in the Globus-M, Nucl. Fusion. **46**(8) (2006) S625.
- [10]. E.O. KISELEV et al., Free-Boundary Plasma Equilibrium Computation in Spherical Globus-M2 Tokamak by Means of the pyGSS Code, Plasma Phys. Rep. **49** (2023) 1560–1577.
- [11]. S.A. GALKIN, et al., Comparison of tokamak axisymmetric mode growth rates from linear MHD and equilibrium evolution approaches, Nuclear Fusion **37** (1997) 1455.
- [12]. E.E. TKACHENKO et al., Plasma Stored Energy Analysis during Neutral Beam Injection in the Globus-M2 Tokamak Using the Pet Equilibrium Code and Diamagnetic Measurements, Plasma Phys. Rep. **49** (2023) 1515–1523.
- [13]. W. ECKSTEIN, Garcia-Rosales C., J. Roth, et al. Sputtering data, MPI-Garching Report IPP-9/82, MPI-Garching, February (1993).
- [14]. J. ROTH and C. GRACIA-ROSALES, Analytic description of the chemical erosion of graphite by hydrogen ions, Nucl. Fusion **36** (1996) 1647.